9/7-6-95
(1) JS

SANDIA REPORT

SAND95-8229 • UC–411
Unlimited Release
Printed June 1995

Large-Solid-Angle Illuminators for Extreme Ultraviolet Lithography With Laser Plasmas

G. D. Kubiak, D. A. Tichenor, W. C. Sweatt, W. W. Chow

Prepared by
Sandia National Laboratories
Albuquerque, New Mexico 87185 and Livermore, California 94551
for the United States Department of Energy
under Contract DE-AC04-94AL85000

UC-411

SAND95-8229
Unlimited Release
Printed June 1995

LARGE-SOLID-ANGLE ILLUMINATORS FOR EXTREME ULTRAVIOLET LITHOGRAPHY WITH LASER PLASMAS

Glenn D. Kubiak and Daniel A. Tichenor
Sandia National Laboratories/CA
Livermore, CA 94551-0969

William C. Sweatt, Weng W. Chow
Sandia National Laboratories/NM
P.O. Box 5800
Albuquerque, NM 87185-0980

ABSTRACT

Laser Plasma Sources (LPSs) of extreme ultraviolet radiation are an attractive alternative to synchrotron radiation sources for extreme ultraviolet lithography (EUVL) due to their modularity, brightness, and modest size and cost. To fully exploit the extreme ultraviolet power emitted by such sources, it is necessary to capture the largest possible fraction of the source emission half-sphere while simultaneously optimizing the illumination stationarity and uniformity on the object mask. In this LDRD project, laser plasma source illumination systems for EUVL have been designed and then theoretically and experimentally characterized. Ellipsoidal condensers have been found to be simple yet extremely efficient condensers for small-field EUVL imaging systems. The effects of aberrations in such condensers on extreme ultraviolet (EUV) imaging have been studied with physical optics modeling. Lastly, the design of an efficient large-solid-angle condenser has been completed. It collects 50% of the available laser plasma source power at 14 nm and delivers it properly to the object mask in a wide-arc-field camera.

I. Introduction

Extreme ultraviolet lithography (EUVL) is an all-reflective lithographic patterning method that is being developed to mass-produce integrated circuits having a minimum linewidth of ≤ 0.13 μm[1]. A schematic diagram of the method is shown in Fig. 1. As in any lithographic method, the radiation (e.g. photons, electrons, or ions) produced by a source is collected and directed to an object mask bearing the structure that is to be imprinted on a resist-coated silicon wafer. An image of the object mask is then cast onto the wafer to chemically transform the resist in some way, thus forming a patterned replica of the mask. In EUVL, photons with $\lambda \sim 14$ nm can be generated by a laser-produced plasma, synchrotron orbital ring, or electrical discharge source. This radiation must be collected with a high efficiency condenser and then delivered to a reflective object mask. The radiation reflected from the mask is finally projected with some reduction factor (typically between 4x - 20x) onto the wafer. Obviously, to reduce lithographic costs, the throughput of properly exposed wafers should be as high as possible. Thus, the illumination system must extract the maximum fraction of emitted source power and simultaneously achieve precise and uniform illumination of the object mask. The goal of this LDRD was to develop and characterize such systems.

Ia. Sources

Sandia National Laboratories and AT&T Bell Laboratories are working together to develop an EUVL tool. We are considering two sources of EUV light: LPSs and synchrotrons. The LPS seems to be the better choice because of its efficiency, size, and cost. The plasma is produced by a high power, pulsed-laser that is focused on a metal (Au, Sn, W...) or cryogenic solid (Xe, Kr, H_2O) surface. This plasma radiates approximately as a blackbody radiator at a temperature of ~200,000 K, converting approximately 1-2% of the incident laser energy into EUV radiation within the desired spectral bandwidth. The plasma also ablates, melts, and shocks the target, producing unwanted high-velocity ejecta debris that can damage or coat the collecting mirror. The production of such debris must be eliminated before the LPS can be used in a commercial tool. Several new target schemes involving cryogenic solids look quite promising[2,3] in this regard.

Ib. Illuminators in General

The condenser is an important component of a projection imaging system, and it can affect image quality as well as exposure time.[4] The condenser system must uniformly illuminate the mask (±1%) with partially coherent light. Both requirements can be satisfied with a Köhler illumination geometry. In Köhler illumination, an incoherent source is imaged into the entrance pupil. The illumination is partially coherent if the ratio of the source image diameter to the entrance pupil diameter, $\sigma = D_{source}/D_{pupil}$, is less than unity; $50\% \leq \sigma \leq 60\%$ is typical. This beam must be delivered in such a manner that the direction of the illumination beam on the mask is the same for all field points. Optimal image resolution and contrast will be achieved only if this latter condition, known as stationarity, is satisfied.

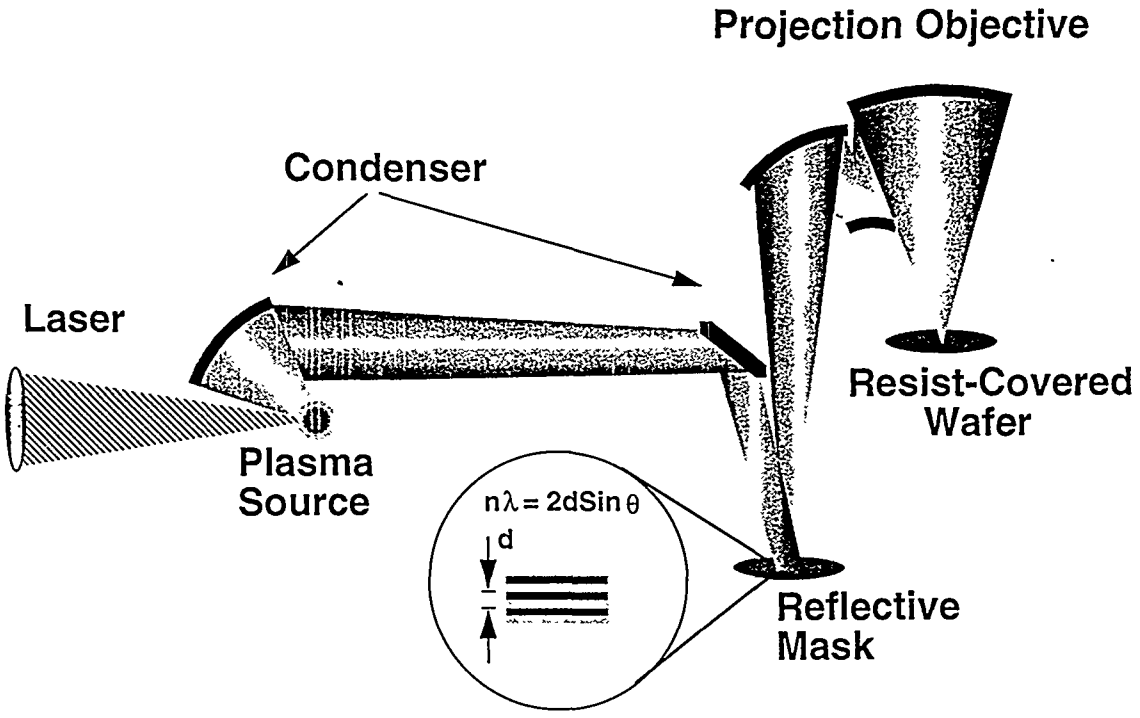

Figure 1. Schematic diagram of an extreme ultraviolet lithography system.

II. Small-Field Schwarzschild Camera

IIa. Condenser for Small-Field Schwarzschild Camera

An off-axis ellipsoidal condenser has been designed and fabricated for use with a 20x Schwarzschild imaging camera. It collects EUV radiation from the LPS and illuminates a transmission mask that is imaged by the Schwarzschild camera onto a resist-coated wafer (See Fig. 2). The condenser is located 250 mm from the LPS and reflects the EUV vertically upward at 90 degrees to the incoming rays. The ellipsoidal condenser is designed to produce a 6x-magnified image of the LPS in the Schwarzschild entrance pupil, which is located non-concentric (decentered) with respect to the mechanical axis to avoid the central obscuration. The resulting coherency factor (σ) is 0.5, based on the half-max diameter of the LPS. Since the brightness of the LPS decreases continuously with increasing radius away from the plasma centroid, the partial coherence produced by this source-condenser system may differ somewhat from that produced by a uniformly bright disk source of the same radius.

Figure errors in the ellipsoidal reflector were measured by introducing a focused HeNe laser beam at the object-plane focal point f_1 and observing the image (the point-spread function) at the image-plane focal point f_2. Ray aberrations as large as 18% of the 0.08 numerical-aperture (NA) entrance-pupil radius were observed. The largest aberrations were in the sagittal direction (out of the plane of Fig 2). Tangential (in plane) condenser aberrations were 5% of the entrance-pupil radius. Condenser aberrations of this magnitude may affect image quality, although they did not appear to be the limiting factor in these experiments due to the much larger figure errors in the imaging optics, as discussed below.

Alignment errors also introduce aberrations in the illuminating wavefront. In order to achieve an accurate alignment, the object-plane focal point f_1 of the ellipsoidal condenser is located on a test bench with a HeNe laser. A 2.5-mm aperture is attached to the condenser to function as a bore sight. The aperture is centered on a line from f_1 to the center of the condenser and located at an axial distance of 20 mm in front of f_1. When the condenser with attached bore sight is placed in the experimental chamber, visible emission from the LPS casts a shadow of the bore sight onto an aperture plate covering the condenser. Lateral alignment is achieved to an accuracy of about $\pm$ 0.5 mm by centering the shadow on the aperture plate. Finally, the axial position of the condenser is adjusted for best focus of the EUV radiation on a scintillating screen at the entrance pupil of the Schwarzschild. This simple alignment scheme is accurate enough to assure that the condenser aberrations due to alignment errors do not exceed those due to figure errors.

IIb. Imaging Results with Small-Field Schwarzschild Camera

Lithographic imaging of positive and negative tone resists at 13.9 nm was performed with the LPS and the multilayer-coated ellipsoidal condenser, as is described more fully in Refs. 5 and 6. Exposures were made using an NA of 0.08, corresponding to a coherent cut-off spatial frequency of 5700 l/mm. As is discussed in Ref. 5, the imaging performance of the Schwarzschild camera was strongly dependent upon the orientation of

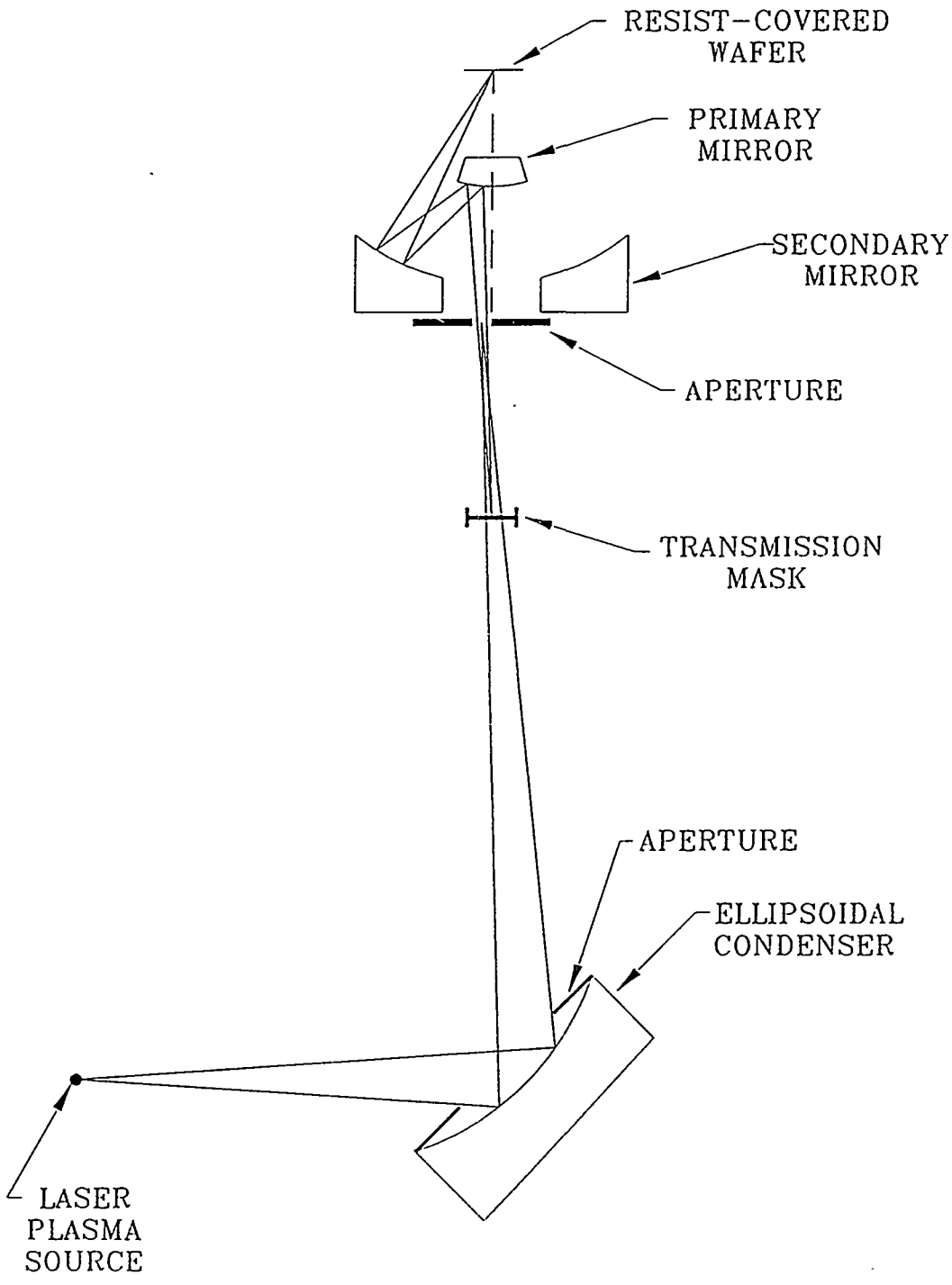

Figure 2. Schematic diagram of small-field EUVL system with laser plasma source, ellipsoidal condenser, and Schwarzschild camera for printing with 20x reduction.

the printed features with respect to the tangential and sagittal directions of the camera. Grating patterns aligned with the good sagittal focus were marginally resolved in PMMA to 0.1 μm.

Figure 3 shows a scanning electron micrograph (SEM) of a resolution test pattern printed in PMMA at 13.9 nm using partially coherent illumination. As can be seen, the grating structures oriented in the sagittal direction are resolved to 0.10 μm, whereas those oriented in the tangential direction are not well-resolved even for the coarsest 0.50 μm features. The off-axis illumination used in the Schwarzschild causes astigmatic imaging, but this alone can not explain the poor performance in the tangential direction. Even at the best tangential focus, 0.15 μm lines and spaces were not well resolved. We attribute this effect to zonal errors seen in interferograms of the aligned Schwarzschild, which yield highly non-axisymmetric optical path differences with respect to the chosen circular subaperture[5]. A higher magnification view of the lower-right quadrant of an image acquired under identical conditions as that shown in Fig. 3 is shown in Fig. 4. As can be seen, the 0.15 μm lines and spaces are recorded with high contrast, but the 0.10 μm features are less well defined. Fig. 5 shows representative SEM's of images recorded in SAL 601, demonstrating that high-contrast 0.15 mm lines and spaces were obtained for the sagittal direction. Exposure times range from ~ 30 sec for PMMA to ~1 sec for chemically amplified resists such as SAL 601. Images acquired in earlier work with an unoptimized condenser required exposure times that were 30 times longer than these values and yielded imaging artifacts caused by illumination coherence [5]. This demonstrates the clear performance benefit obtained when an optimized condenser system is matched to a specific imaging camera.

III. Intermediate-Field Schwarzschild Camera

IIIa. Condenser for Intermediate-Field Schwarzschild Camera

A new Schwarzschild system has been developed to provide a larger field of view and to improve the quality of both the imaging and condensing optics (See Fig 6). The 10x imaging camera in this system is designed to image 0.1 μm features over a 0.4 mm diameter field of view, a 100-fold increase in area over the 20x system. The field size remains far too small for commercial applications. However, it is large enough for further laboratory development, and the imaging camera retains the simplicity of spherical optical elements which are easier to fabricate and measure. The goal is to qualify this system for use in an LPS-based laboratory stepper for device fabrication experiments.

A dedicated LPS, developed for this system, is driven by a Lambda Physik LPX 250 KrF laser emitting 0.6 Joule, 20 ns pulses at a 200 Hz repetition rate. The target system comprises a tape transport mechanism capable of carrying a 25 μm thick mylar tape coated with 0.1 μm of vapor-deposited copper and 0.5 μm electro-plated tin which functions as a mass-limited target.

The condensing system comprises an on-axis ellipsoidal collector located behind a decentered, 50 mm diameter aperture. The aperture protects the unused portion of the ellipsoid from LPS debris. Three sites can be used on each ellipsoid as new surfaces are required. The condenser is designed to produce a 2 mm diameter image of the 150 μm

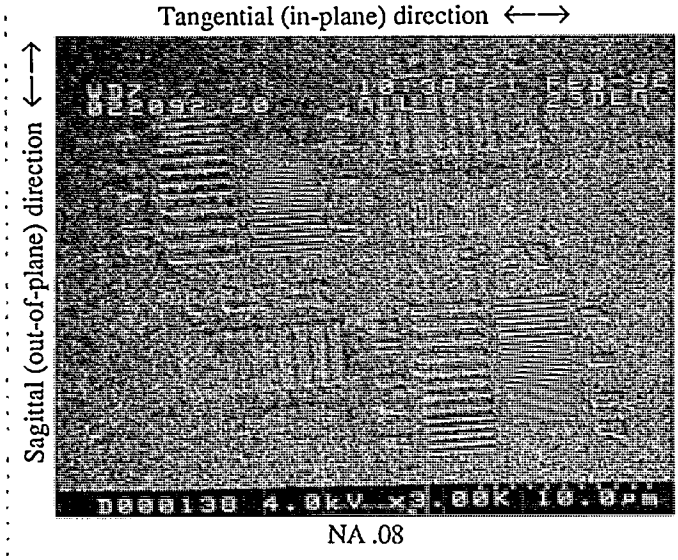

Figures 3. Low-magnification scanning electron micrograph (SEM) of resist patterns printed in PMMA resist with 20x Schwarzschild camera. Grating structures having spatial modulation in the sagittal direction print with higher contrast than gratings with modulation in the tangential direction.

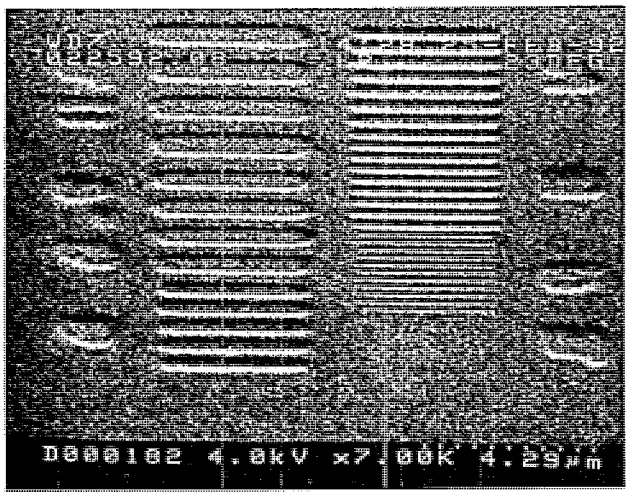

Figure 4. High-magnification SEM view of gratings having spatial modulation in the sagittal direction. The smallest resolved features in the lower right are 0.1 μm lines and spaces.

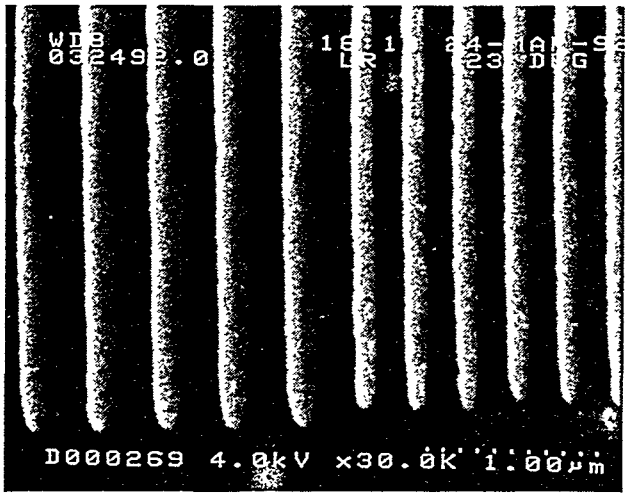

Figure 5. High-magnification SEM view of 0.2 and 0.15 µm lines and spaces patterned in the sagittal direction with the small-field Schwarzschild camera in Shipley SAL 601 negative resist.

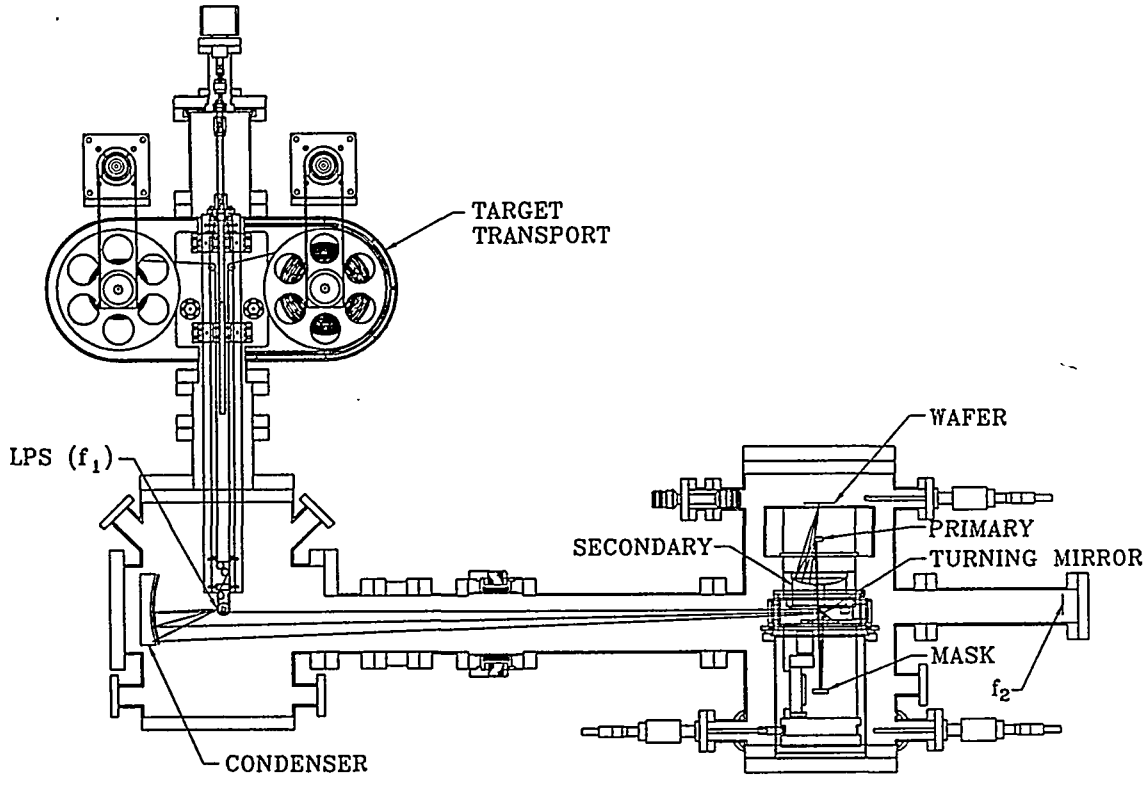

Figure 6. Schematic diagram of 10x EUV imaging system driven by a KrF laser plasma source.

source (13.3 magnification) in the 4 mm entrance pupil of the Schwarzschild for a σ of 0.5. The distance from the LPS to the center of the 50 mm aperture is 112.5 mm, which provides a 0.155 steradian collection solid angle (2.5% of the available 2π steradians). This f/2.25 aperture is sufficient to provide Köhler illumination over the 4 mm field of view in the mask plane. Two ellipsoids have been fabricated having figure errors of $\lambda/6$ and $\lambda/8$ wave (λ = 6328 Å) throughout the 110 mm clear aperture, greatly reducing the condenser aberrations below those present in the 20x system. A 45° turning mirror is required to illuminate a reflecting mask as shown in Fig. 6.

The effects of ellipsoidal condenser aberrations and source partial coherence on the imaging performance have been modeled with the physical optics modeling codes, as described in more detail in references 7 and 8. Specifically, the effects of condenser coma and astigmatism are found to significantly degrade EUV images only for figure departures of $\geq 2\ \lambda$ (for λ = 14 nm). This important result establishes that the figure accuracy that EUVL condenser systems must achieve is approximately 20 times more forgiving than that required for the optical elements in the imaging camera itself.

IIIb. Imaging Results with Intermediate-Field Schwarzschild Camera

Imaging performance of the Schwarzschild camera was established with a reflective mask containing various test patterns to produce printed features ranging in size from 5 μm to 0.05 μm. The mask is a Mo/Si multilayer-coated fused silica flat patterned with a bilayer absorber having 60 nm of hard baked resist and 30 nm of Ge. Figs. 7-9 show scanning electron micrographs (SEMs) of selected test structures located on the mask. Fig. 7(b) shows a spoke-pattern resolution target used to reveal astigmatism, Fig. 8(b) shows equal line/space gratings with pitch of 3 μm and 2 μm, Fig. 9(b) shows gate/pad structures with gate widths of 1.5 μm and 1 μm, and Fig. 9(d) shows gratings with pitch ranging from 6 - 2 μm. Masks have been fabricated in both light- and dark-field tones; all results presented here were obtained with the light-field mask.

Exposures were performed in the positive-tone resists poly(methyl methacrylate) (PMMA) (OCG Microelectronics) and ZEP 520 (Nippon Zeon). Initial resist exposures were performed with no additional spectral filtering. In this case, ~500 laser pulses were required to clear 70 nm of PMMA, yielding strong modulation at 0.1 μm. Imaging artifacts caused by the presence of unwanted long-wavelength radiation grew increasingly noticeable over the course of many exposures, especially in ZEP. We attribute this to a reduction in the spectral contrast at 13.4 nm caused by the deposition of plasma source debris on the condenser. Si membranes 0.38 μm thick were used to remove unwanted spectral components, increasing the necessary exposure time by a factor of 2 but sharply increasing printed image contrast, as expected. Spectral purity was not an issue in our earlier 20x system because a transmissive Si membrane mask was used, providing adequate filtering of long-wavelength components for all but the most visible-light-sensitive resists.

Typical images recorded in ZEP are shown in the SEMs of Figs. 7-9 These images and others recorded in PMMA exhibit reasonable two-dimensional image fidelity across the full design exposure field of 0.4 mm to a resolution of ~0.2 μm, although image contrast decreases sharply for smaller structures. For example, Fig. 7(a) shows no discernable astigmatism down to 0.2 μm, while the 0.1 μm lines and spaces shown on the

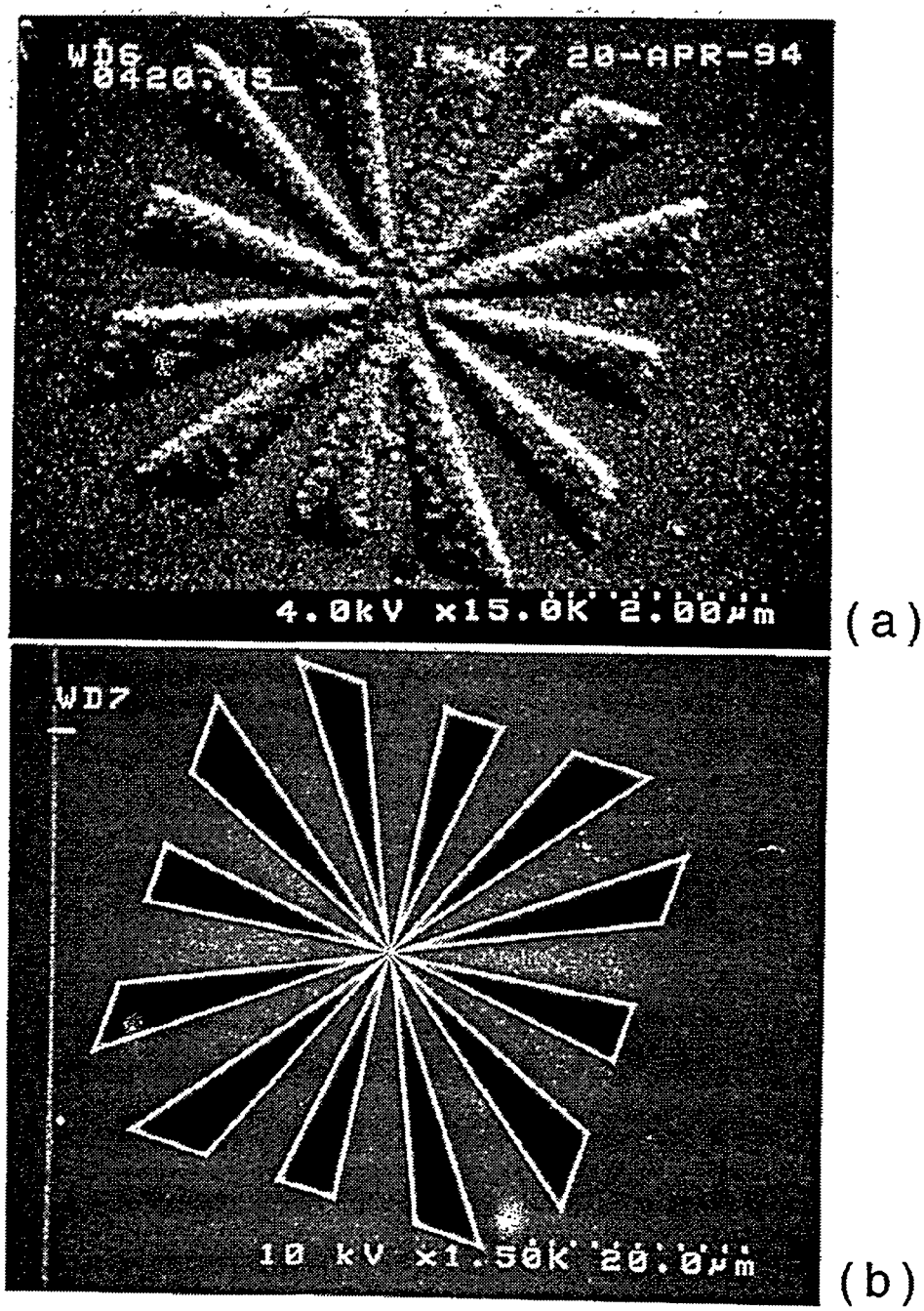

Figure 7. SEM of a star resolution target on the reflective mask (b), and its resulting image printed at 13.4 nm in ZEP 520 (a). The SEM of the resist pattern in the top panel was obtained with the sample rotated 26° with respect to the electron beam to improve SEM contrast. No rotation was applied to obtain the SEM of the mask.

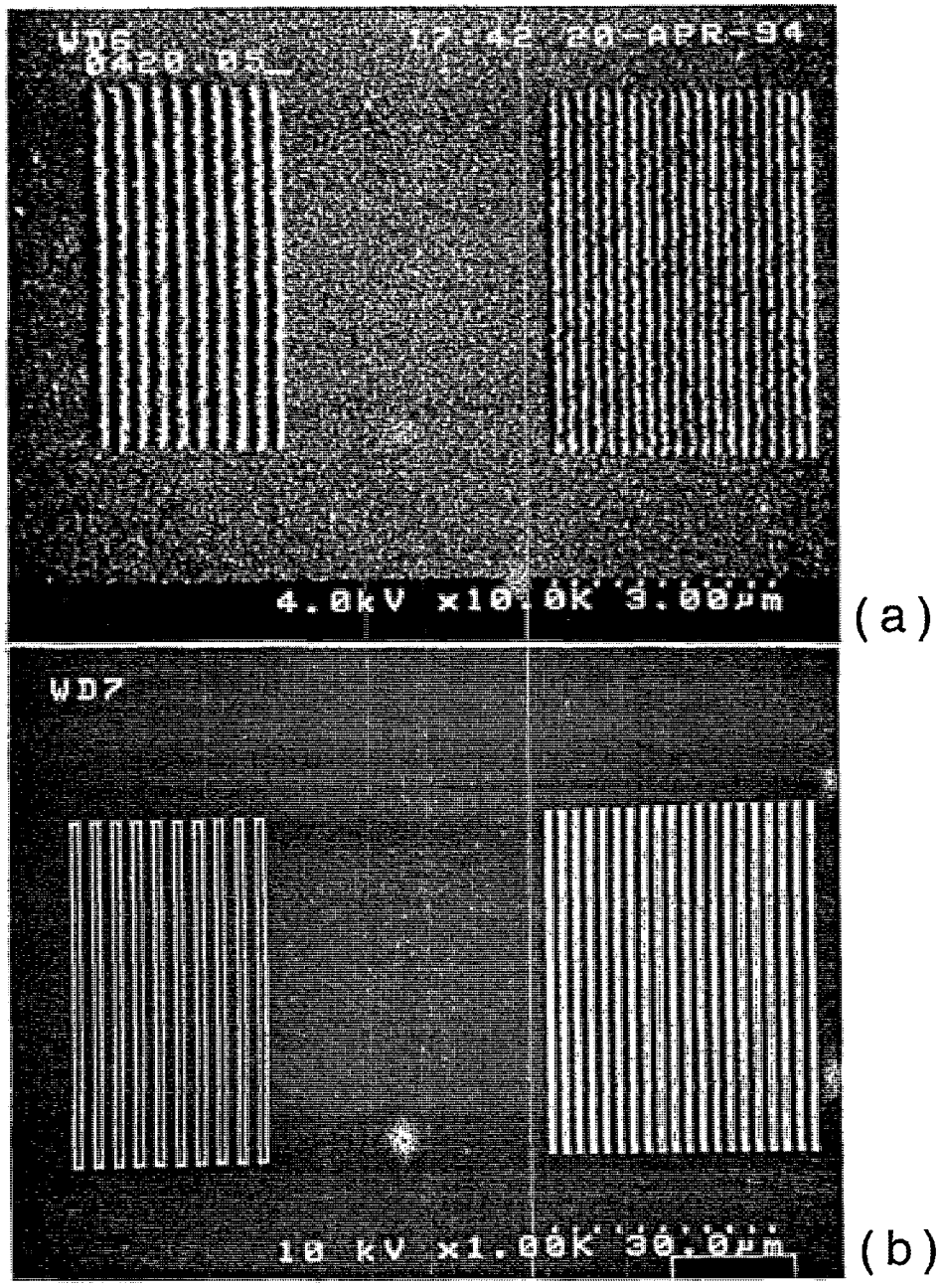

Figure 8. SEMs of 1.5 µm (left) and 1.0 µm (right) line/space grating resolution targets on the reflective mask (b), and their corresponding images printed at 13.4 nm in ZEP 520 (a). The nominal printed resist linewidths are 0.15 µm (left) and 0.1 µm (right). The SEM of the resist pattern in the bottom panel was obtained with the sample rotated 26° with respect to the electron beam to improve SEM contrast. No rotation was applied to obtain the SEM of the mask.

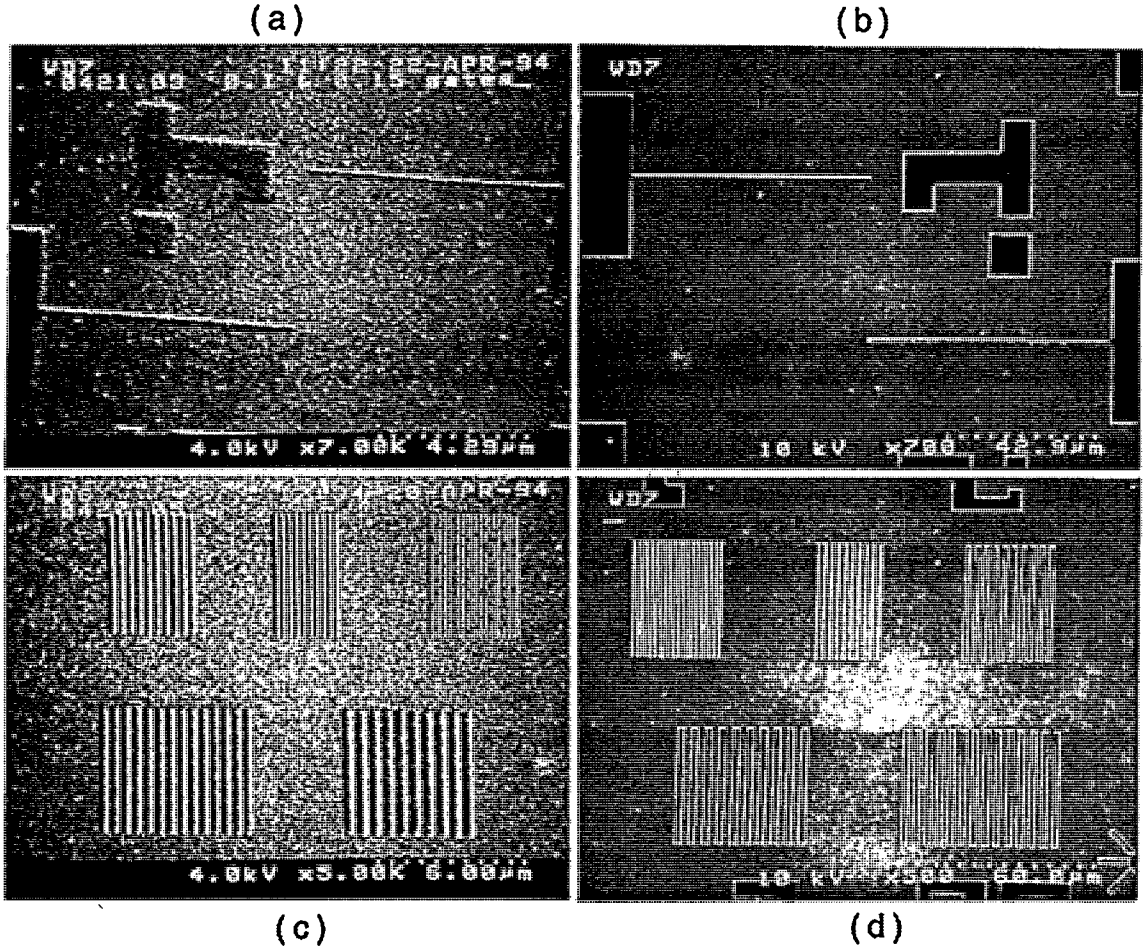

Figure 9. SEMs of 1.0 µm and 1.5 µm gate resolution targets (b) and equal line/space gratings (d) on the reflective mask and their corresponding images printed at 13.4 nm in ZEP 520, (a) and (c). SEMs of the resist patterns in (a) and (c) were obtained with the samples rotated 26° with respect to the electron beam to improve SEM contrast. No rotation was applied to obtain the SEMs of the mask.

right in Fig. 8(a) are marginally resolved in ZEP and are only slightly better in PMMA. Imaging artifacts associated with highly coherent illumination, such as speckle and ringing, are not observed. These images are consistent with the 2 nm WFE measured for the camera after final alignment and are substantially improved over images produced with the 20x Schwarzschild shown in Figs. 3-5, due to zonal errors present in the mirror substrates of this early system. Further improvements in image quality are expected from other mirror pairs which were fabricated at the same time as the pair used in this work but which have slightly improved figure. These optics are to be incorporated in a laboratory EUVL tool based on the 10x Schwarzschild camera and a magnetically levitated fine-control stage for precise wafer positioning. This system is currently under construction and will provide the capability for future device fabrication.

IV. Condenser for Scanning Ring-Field Camera

Ring-field cameras can be designed to be aberration-free at a given radius, i.e., R_{image} = *25 mm ± ~1 mm.* A 60° arc at this radius gives a 25-mm chord length. Large chips (25-mm square) can be printed with such a camera if the mask and wafer are scanned perpendicular to this chord. An example design[9] is shown in Figure 10. Note that the mask is reflective, so the entrance pupil has to be virtual.

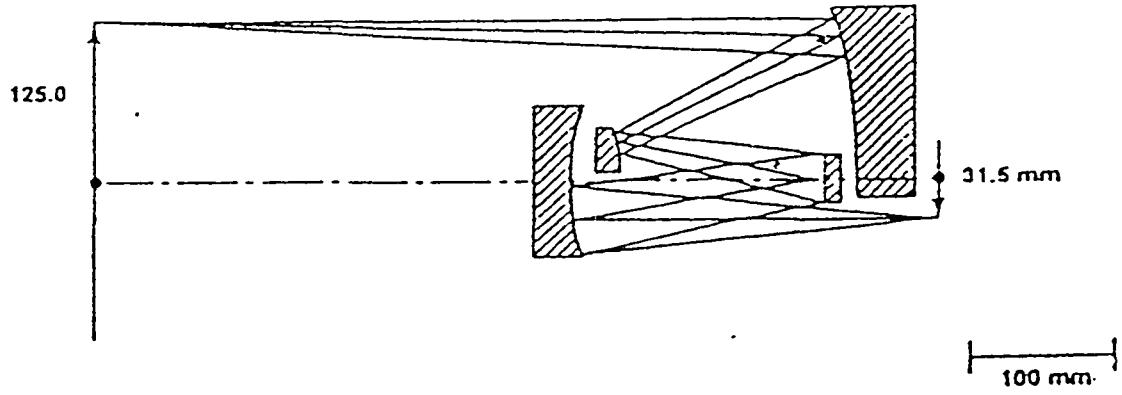

Figure 10. Schematic diagram of a four-element ring-field EUVL camera.

A condenser that couples EUV radiation from an LPS into a scanning, ring-field camera was designed. Several candidate schemes for illuminating the scanning-field EUVL imaging camera were considered, however. Due to their inefficiency and large size, we rejected condenser system designs in which the plasma-facing elements were simple metal-coated grazing incidence mirrors whose illumination efficiency would not be significantly degraded by the deposition of metal (e.g. Au, Ta, or W) plasma debris.

Instead, a design based on a combination of multilayer-coated and grazing incidence mirrors was chosen. This design produces Köhler illumination so the intensity is uniform and some degree of partial coherence can be introduced. The LPS condenser can collect half of the EUV radiation from a 200-μm-diameter LPS if, at the wafer, the ring-field width is $\Delta r \approx 3.5$ *mm.*

Our condenser design gives Köhler illumination in the circumferential direction and what is known as critical illumination in the radial direction. This means that the source is imaged in the slit in the radial direction and crudely imaged into the entrance pupil in the sagittal direction. Thus the intensity along the slit is uniform and fortunately, the scanning smooths out any radial intensity fluctuations.

In this condenser design, the entrance pupil is illuminated with five images of the plasma ball arranged in a pentagon. We center this pentagon in the pupil so the partial coherence is almost radially symmetric. We have designed a similar beam arrangement for the synchrotron condenser.[10]

The condenser for injecting EUV light from the LPS into a ring-field camera has five parallel channels, each composed of three parts: a collector mirror, a beam-rotating roof-mirror pair, and a pupil reimaging mirror. We begin by describing the collector mirrors.

A sketch of the rotationally symmetric "parent" collector mirror is shown in Figure 11. The parent, which might be described as an elliptical axicon, images the "point-source" LPS into a ring. As shown in the figure, five 60° segments are cut from the parent mirror. Each of these segments creates a 60° arc image of the LPS. These arc images have the same shape as the 60° ring field of the camera.

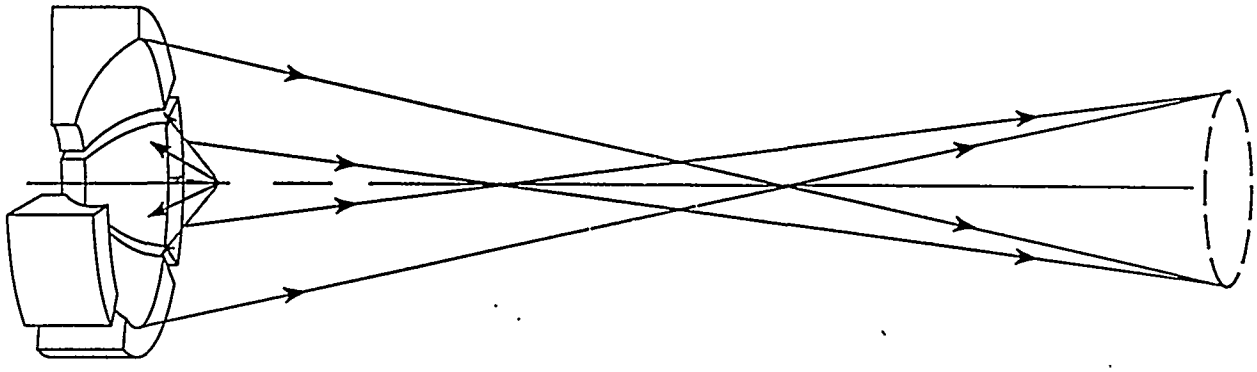

Figure 11. Parent mirror imaging the laser plasma source into a ring.

The rest of the condenser system has to do three things: 1) the arc images have to be individually rotated so they can all be superimposed in the ring field, 2) all five beams have to be squeezed into a real pupil, and 3) this real pupil has to be imaged into the virtual entrance pupil of the camera.

Figure 12 is a sketch of the journey of one beam through the whole system. After departing from the collector mirror, the beam encounters an off-axis, roof-mirror pair. This unit rotates the beam so the arc image fits into the ring field. Five of the roof-mirror pairs, the near-normal mirrors, are arranged in a minimum-sized, quasi-symmetrical array (Figure 12). This is the "real pupil," imaged into the virtual entrance pupil of the camera by the diagonal mirror located just below the reflective mask. This mirror will have an elliptical surface and will be about F/15.

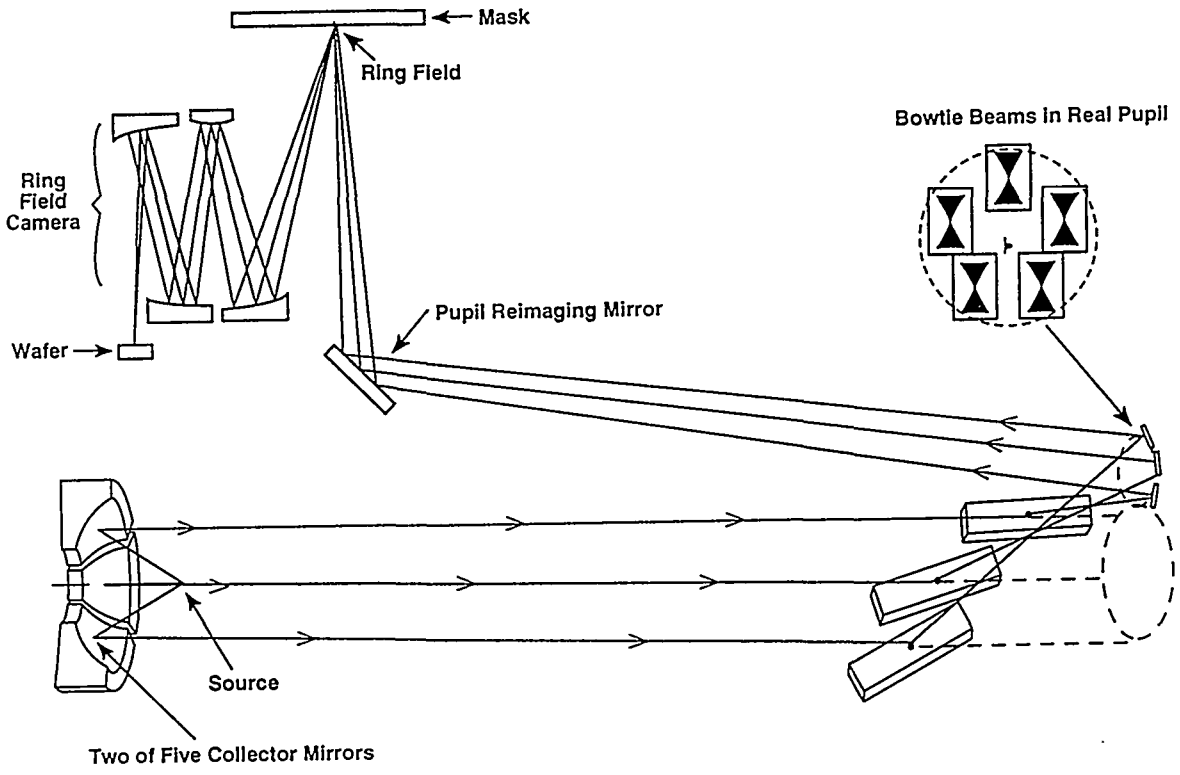

Figure 12. Schematic diagram of the condenser system showing the optical path from the laser plasma source through the condenser system to the object mask, ring-field camera and wafer.

The system efficiency is maximized by locating the real pupil where the beam segments are smallest; hence, they can be packed into the smallest array. Figure 11 shows this location to be where the middle ray in the bowtie-shaped, beam segment crosses the axis.

We see in Figure 11 that the beams are overlapped, so the five mirror segments must be tilted outward. We tilt them until the central rays in the five beams are parallel. These segment center lines form a pentagon, and we want to translate them into another pentagon in the real pupil. Figure 13 shows a mapping of the input pentagon into the real-pupil pentagon that incidentally gives the desired rotation of the arc images, sketched for both the input and output beams. Note that the desired rotation angle for each beam is exactly twice that of the connecting ray, which is the precise function of a roof mirror.

The simple geometry just described succeeds when the input and output beams are parallel. As shown in Figure 12, the output beam has a small upward tilt that was added so two of the output beams would not run into the upper collector mirrors. This deviation from parallelism requires that all of the mirrors be slightly tipped and tilted from the orientations that would be used for the "simple geometry." The grazing mirrors also need to be translated slightly.

In the roof-mirror pair, the first mirror is used at grazing incidence and the second one is near normal. This placement allows the beams to be tightly packed in the real pupil. A rhodium-coated, grazing-incidence mirror also happens to have higher reflectivity than would a near-normal multilayer. For an angle of incidence of 80°, the reflectivity is $R_{Rh@80} = 85\%$.

V. Modeling of the Laser Plasma Source Condenser and its Implications

Physical optics modeling has been performed to validate the design concept of the LPS condenser. The mask shown in Figure 14a is well imaged using a source composed of five-point sources[11]. Figure 14b shows good imagery with only modest ringing. Figure 14c is an image of the same mask using partially coherent, disk illumination. Note that Figures 14b and 14c are quite similar. We will soon model the five bowties to see if the array should be symmetric or slightly elliptical. We also need to know the size of the pentagon in the entrance pupil. This size affects the condenser efficiency, which will be addressed in the next discussion.

The étendue or Lagrange invariant of the camera limits the étendue of the condenser, and hence its efficiency. The étendue of the camera in the radial direction is

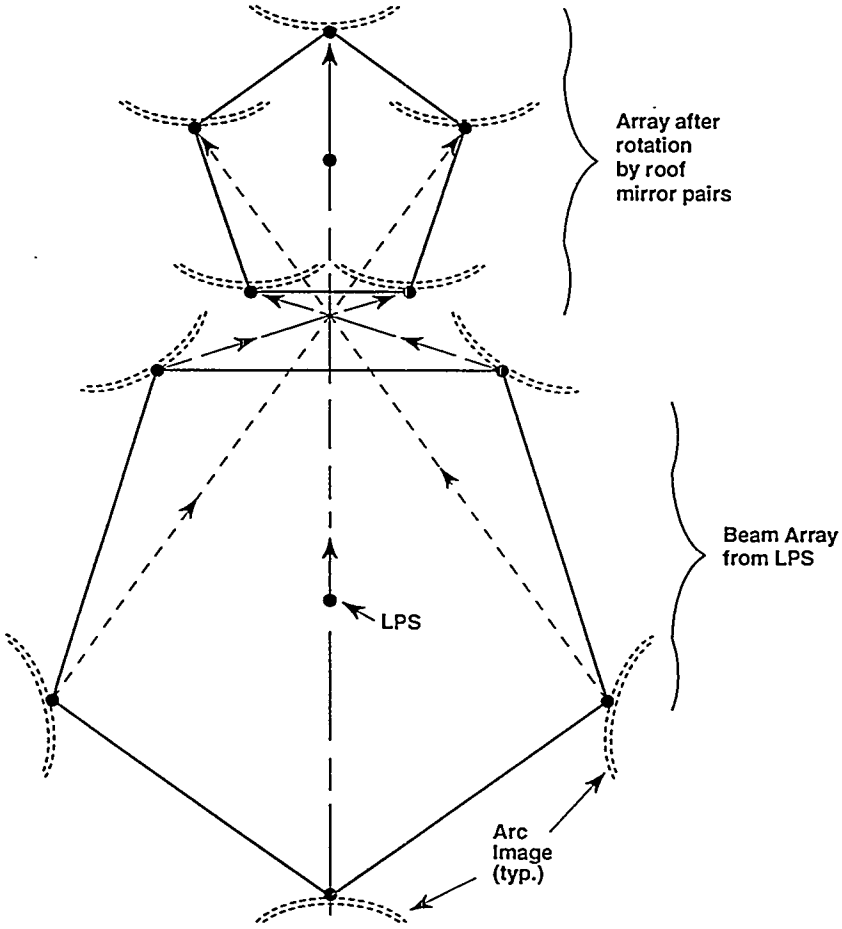

Figure 13. Beam rotation and translation geometry.

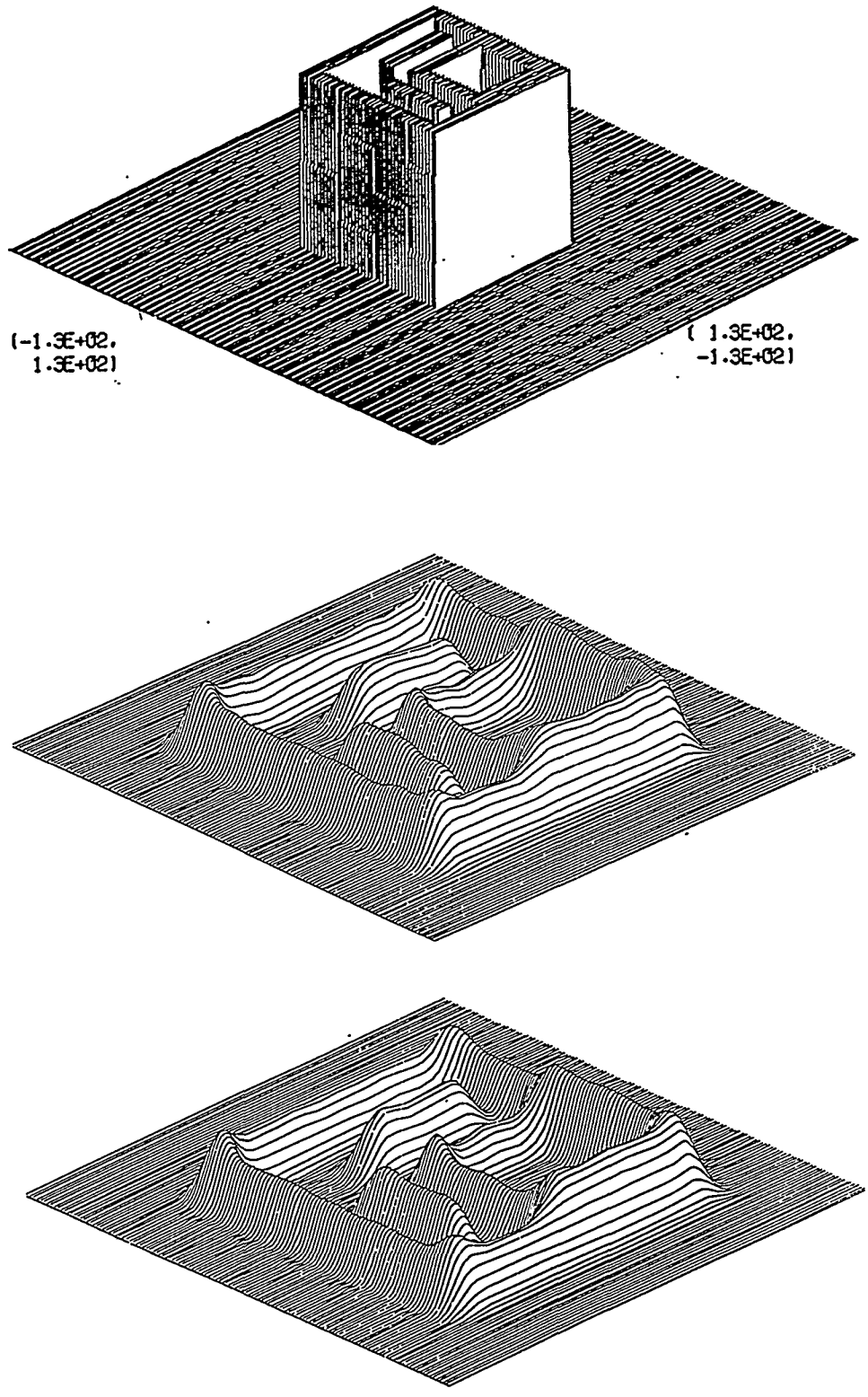

Figure 14. (a) Object pattern to be imaged by the EUVL system; (b) Image of the object shown in (a) when imaged with illumination provided by five point sources arranged in a pentagon; (c) Image of the object shown in (a) when imaged with partially coherent illumination ($\sigma = 0.5$).

the product of the numerical aperture, n.a. = 0.10, and the slit width, Δr_{image}. The étendue of the condenser is further reduced by the pupil fill factor, $\sigma = 0.5$. Furthermore, five segments must fit in the array so the beam segments must be 44% smaller. The étendue of one beam is

$$E_{condenser} \leq 44\% * \sigma * n.a._{image} * \Delta r_{image} = 0.022 * \Delta r_{image}$$

At the source, the étendue is approximately $E_{LPS} \approx D_{LPS} * \Delta\phi$,where D_{LPS} is the diameter of the plasma ball and $\Delta\phi = \phi_{max} - \phi_{min}$ is the collection angle. This can be set equal to the étendue of the condenser, so the collection angle is limited by the function

$$\Delta\phi \leq 0.22 * (\Delta r_{image} / D_{LPS})$$

The condenser efficiency increases with $\Delta\phi$, so it also increases with the slit width and decreases as the plasma ball grows.

The étendue is a first-order property and the collection angles are large, so the last equation is only an approximation. Figure 15 is the output of a more accurate calculation of the efficiency. It includes the effects of aberrations in the collector mirror, vignetting at the slit, reflectivity losses, and an experimentally determined[12], non-Lambertian source radiance. The three curves are for different maximum collection angles, ϕ_{max}. A spherical LPS with $D_{LPS} = 200\ \mu m$ has been assumed.

Because of these calculations, the brightness of the LPS is now being optimized, in addition to its efficiency. Also, since it is evident that a wider camera slit would be better, we are striving to increase it from $\Delta r_{present} = 1\ mm$ to $\Delta r_{goal} \geq 2.5\ mm$.

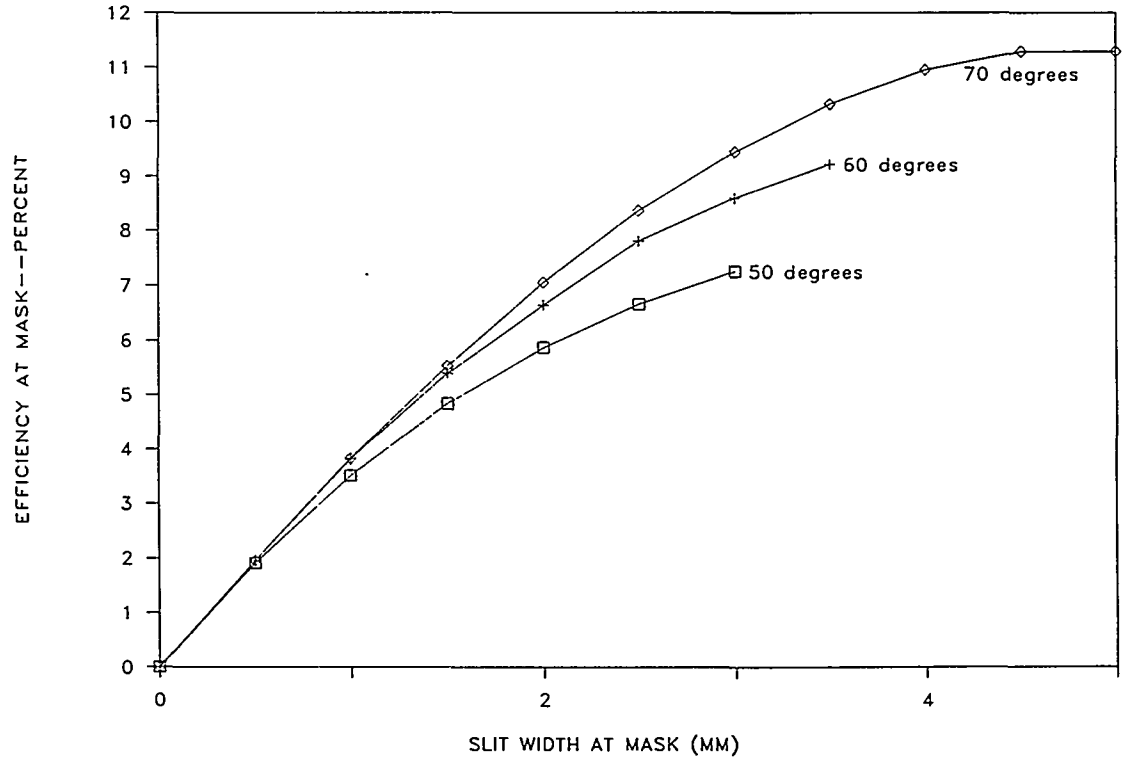

Figure 15. Laser plasma source condenser efficiency vs. slit width, Δr_{image}, with $D_{LPS} = 200\ \mu m$.

VI. Summary

Reflective condenser systems that collect a large solid angle of EUV radiation emitted from laser-produced plasma sources have been designed, theoretically analyzed, fabricated, and experimentally characterized for EUVL applications. These condensers have evolved from simple, single-surface ellipsoids to segmented, multielement axicon-based systems as imaging system field areas have grown from ~$1x10^{-3}$ mm^2 in the early experimental camera to 625 mm^2 in the advanced production-worthy scanning ring-field EUVL camera. During this evolution, the fundamental condenser figure requirements have been theoretically examined and are now understood to be approximately an order of magnitude less precise than those of the imaging camera mirror elements. A condenser design has been presented that couples a laser plasma source to a ring-field lithography camera. This system can deliver 10% to 12% of the LPS flux to the mask with properties of very good intensity uniformity and reasonable partial coherence. Assuming that this condenser can be fabricated, aligned and illuminated with an EUV source of sufficient power, it would be capable of meeting the needs of a production-worthy lithography system for the fabrication of integrated circuits. Advances in the fabrication of precision aspheric camera mirrors, the development of low-distortion fixturing of camera elements, and the development of high-power, "zero-debris" EUV sources, will be required before this can occur, however. As a result of this and other LDRDs, many of these issues are being addressed now through the auspices of the DOE-funded EUVL program at Sandia/California, Sandia/New Mexico, Lawrence Livermore National Laboratory, Los Alamos National Laboratory, and other laboratories.

VII. References

1. Kinoshita, et al., "Soft X-Ray Reduction Lithography-Using Multilayer Mirrors," J. Vac. Soc. Technol. **B7** 1648 (1989); J. E. Bjorkholm, et al., "Reduction Imaging at 14 mm Using Multilayer-Coated Optics: Printing of Features Smaller than 0.1 μm," J. Vac. Soc. Technol. **B8** 1509-1513 (1990).
2. G. D. Kubiak, K. W. Berger, S. J. Haney, P. D. Rockett, and J. A. Hunter, OSA Proceedings on Soft X-Ray Projection Lithography **18**, 127 (1993)
3. M. C. Richardson, K. Gabel, F. Jin, and W. T. Silfvast, OSA Proceedings on Soft X-Ray Projection Lithography **18**, 156 (1993)
4. D. S. Goodman, "Lithographic image simulations," Microelectron. Eng. **3**, 355 (1985).
5. D. A. Tichenor, G. D. Kubiak, M. E. Malinowski, R. H. Stulen, S. J. Haney, K. W. Berger, L. A. Brown, W. C. Sweatt, J. E. Bjorkholm, R. R. Freeman, M. D. Himel, A. A. MacDowell, D. M. Tennant, O. R. Wood, II, J. Bokor, T. E. Jewell, W. M. Mansfield, W. K. Waskiewicz, D. L. White and D. L. Windt, Appl. Optics **32**, 7068 (1993)
6. G. D. Kubiak, D. A. Tichenor, W. W. Chow, W. C. Sweatt, and M. D. Himel, Proc. of the SPIE **1924,** 18 (1993).
7. D. A. Tichenor, G. D. Kubiak, M. E. Malinowski, R. H. Stulen, S. J. Haney, K. W. Berger, R. P. Nissen, G. A. Wilkerson, P. H. Paul, S. R. Birtola, P. S. Jin, R. W. Arling, A. K. Ray-Chaudhuri, W. C. Sweatt, W. W. Chow, J. E. Bjorkholm, R. R. Freeman, M. D. Himel, A. A. MacDowell, D. M. Tennant, O. R. Wood, II, W. K. Waskiewicz, D. L. White, D. L. Windt and T. E. Jewell, "Development of a laboratory extreme ultraviolet lithography tool," Proc. SPIE **2194**, 95 (1994).
8. G. D. Kubiak, D. A. Tichenor, A. Ray-Chaudhuri, M. E. Malinowski, R. H. Stulen, S. J. Haney, K. W. Berger, G. A. Wilkerson, P. H. Paul, J. E. Bjorkholm, L. A. Fetter, R. R. Freeman, M. Himel, T. E. Jewell, A. A. MacDowell, D. M. Tennant, W. K. Waskiewicz, D. L. White, D. L. Windt, and O. R. Wood, II, "Characterization of an Expanded-Field Schwarzschild Objective for Extreme Ultraviolet Lithography," Journ. Vac. Sci. and Technol. **B 12**, 3820 (1994).
9. T. E. Jewell, J. Vac. Sci. Technol. **B8** 1519-1523 (1990).
10. W. C. Sweatt and G. N. Lawrence, "Physical optics modeling in soft x-ray projection lithography," Appl. Optics **32**, 6945 (1993).
11. W. C. Sweatt and G. N. Lawrence, "Image Degradation in an SXPL System Due to Diffraction Phenomena," OSA An. Mtg., Albuquerque, NM (1992).
12. P. D. Rockett, Sandia National Laboratories, Private Communication, Dec. 7, 1993.

APPENDIX A — List of publications, presentations, patents, and invention disclosures

Publications :

1. G. D. Kubiak, R. Q. Hwang, M. T. Schulberg, E. M. Kneedler, K. W. Berger, J. E. Bjorkholm, and W. M. Mansfield, "Characterization of chemically amplified resists for soft x-ray projection lithography," J. Vac. Sci. Technol. **B10**, 2593-2599 (1992).

2. D. A. Tichenor, G. D. Kubiak, M. E. Malinowski, R. H. Stulen, S. J. Haney, K. W. Berger, L. A. Brown, W. C. Sweatt, J. E. Bjorkholm, R. R. Freeman, M. D. Himel, A. A. MacDowell, D. M. Tennant, O. R. Wood, II, J. Bokor, T. E. Jewell, W. M. Mansfield, W. K. Waskiewicz, D. L. White and D. L. Windt, "Soft-x-ray projection lithography experiments using Schwarzschild imaging optics," Appl. Optics **32**, 7068 (1993).

3. S. J. Haney, K. W. Berger, G. D. Kubiak, P. D. Rockett, and J. Hunter, "Prototype High-Speed Tape Target Transport for a Laser Plasma Soft X-Ray Projection Lithography Source," Appl. Optics **32**, 6934 (1993).

4. G. D. Kubiak, R. Q. Hwang, M. T. Schulberg, D. A. Tichenor, and K. Early, "Chemically Amplified Soft X-Ray Resists: Sensitivity, Resolution, and Molecular Photodesorption," Appl. Optics **32**, 7036 (1993).

5. W. C. Sweatt and G. N. Lawrence, "Physical optics modeling in soft x-ray projection lithography," Appl. Optics **32**, 6945 (1993).

6. D. A. Tichenor, G. D. Kubiak, M. E. Malinowski, R. H. Stulen, S. J. Haney, K. W. Berger, R. P. Nissen, R. L. Schmitt, G. A. Wilkerson, L. A. Brown, P. A. Spence, P. S. Jin, W. C. Sweatt, W. W. Chow, J. E. Bjorkholm, R. R. Freeman, M. D. Himel, A. A. MacDowell, D. M. Tennant, O. R. Wood, II, W. K. Waskiewicz, D. L. White, D. L. Windt and T. E. Jewell, "Development and characterization of a 10x Schwarzschild system for soft-x-ray projection lithography," **OSA Proceedings on Soft X-Ray Projection Lithography**, A. M. Hawryluk and R. H. Stulen, eds., Vol. 18, 79 (1993).

7. W. C. Sweatt, "High-efficiency condenser design for illuminating a ring field," **OSA Proceedings on Soft X-Ray Projection Lithography**, A. M. Hawryluk and R. H. Stulen, eds., Vol. 18, (1993).

8. G. D. Kubiak, K. W. Berger, S. J. Haney, P. D. Rockett and J. A. Hunter, "Laser Plasma Sources for Soft X-Ray Projection Lithography: Production and mitigation of debris," **OSA Proc. on Soft X-Ray Projection Lithography,** A. M. Hawryluk and R. H. Stulen, eds., Vol. 18, 127 (1993).

9. G. D. Kubiak, D. A. Tichenor, W. W. Chow, W. C. Sweatt, and M. D. Himel, "Resist performance in soft x-ray projection lithography," Proc. of the SPIE Symp. on Electron-Beam, X-ray, and Ion-Beam Submicrom. Lithographies for Manuf. III, vol. **1924**, 18 (1993).

10. G. D. Kubiak, K. W. Berger, S. J. Haney, D. A. Tichenor, and R. H. Stulen, P. D. Rockett and J. A. Hunter, "High-Power Laser Plasma Sources: Soft X-Ray Projection Lithography and Other Applications", Proc. of the Conf. on Laser Ablation: Mechanisms and Applications-II, Knoxville, TN, April 1993, AIP Conf. Proc. **288**, 534 (1994).

11. G. N. Taylor, R. S. Hutton, S. M. Stein, C. H. Boyce, B. La Fontaine, A. A. MacDowell, O. R. Wood II, D. R. Wheeler, and G. D. Kubiak, Proc. Microelectronic Engineering **23**, 279 (1994).

12. G. D. Kubiak, D. A. Tichenor, A. Ray-Chaudhuri, M. E. Malinowski, R. H. Stulen, S. J. Haney, K. W. Berger, G. A. Wilkerson, P. H. Paul, J. E. Bjorkholm, L. A. Fetter, R. R. Freeman, M. Himel, T. E. Jewell, A. A. MacDowell, D. M. Tennant, W. K. Waskiewicz, D. L. White, D. L. Windt, and O. R. Wood, II, "Characterization of an Expanded-Field Schwarzschild Objective for Extreme Ultraviolet Lithography," Journ. Vac. Sci. and Technol. **B 12**, 3820 (1994).

13. D. A. Tichenor, G. D. Kubiak, M. E. Malinowski, R. H. Stulen, S. J. Haney, K. W. Berger, R. P. Nissen, R. L. Schmitt, G. A. Wilkerson, P. S. Jin, W. C. Sweatt, W. W. Chow, J. E. Bjorkholm, R. R. Freeman, M. D. Himel, A. A. MacDowell, D. M. Tennant, O. R. Wood, II, W. K. Waskiewicz, D. L. White, D. L. Windt and T. E. Jewell, "Application of laser plasma sources in soft-x-ray projection lithography," **Proc. of the SPIE Symp. on Applications of Laser Plasma Radiation**, vol. 2015, 104 (1994).

14. D. A. Tichenor, G. D. Kubiak, M. E. Malinowski, R. H. Stulen, S. J. Haney, K. W. Berger, R. P. Nissen, G. A. Wilkerson, P. H. Paul, S. R. Birtola, P. S. Jin, R. W. Arling, A. K. Ray-Chaudhuri, W. C. Sweatt, W. W. Chow, J. E. Bjorkholm, R. R. Freeman, M. D. Himel, A. A. MacDowell, D. M. Tennant, L. A. Fetter, O. R. Wood, II,W. K. Waskiewicz, D. L. White, D. L. Windt, and T. E. Jewell, "Development of a Laboratory Extreme-Ultraviolet Lithography Tool," **Proc. of the SPIE Symp. on Electron-Beam, X-Ray, and Ion-Beam Submicrometer Lithographies for Manufacturing IV**, vol. 2194, 95 (1994)

Presentations :

1. Ref. 2 presented at the OSA Topical Meeting on Soft-X-Ray Projection Lithography, Monterey, CA, April 6-8, 1992.

2. D. A. Tichenor, G. D. Kubiak, M. E. Malinowski, R. H. Stulen, S. J. Haney, K. W. Berger, L. A. Brown, W. C. Sweatt, J. E. Bjorkholm, R. R. Freeman, M. D. Himel, A. A. MacDowell, D. M. Tennant, O. R. Wood, II, J. Bokor, T. E. Jewell, W. M. Mansfield, W. K. Waskiewicz, D. L. White and D. L. Windt, "High-resolution soft-x-ray projection imaging using Schwarzschild optics and a laser plasma source," presented at the OSA Annual Meeting, September 20-25, 1992.

3. Ref. 6 presented at the OSA Topical Meeting on Soft-X-Ray Projection Lithography, Monterey, CA, May 10-12, 1993.

4. Ref. 13 presented at the SPIE Conference on Applications of Laser Plasma Radiation, San Diego, CA, July 14-16, 1993.

5. D. A. Tichenor, G. D. Kubiak, M. E. Malinowski, R. H. Stulen, S. J. Haney, K. W. Berger, R. P. Nissen, R. L. Schmitt, G. A. Wilkerson, P. S. Jin, W. C. Sweatt, W. W. Chow, J. E. Bjorkholm, R. R. Freeman, M. D. Himel, A. A. MacDowell, D. M. Tennant, O. R. Wood, II, W. K. Waskiewicz, D. L. White, D. L. Windt and T. E. Jewell, "A 10x Schwarzschild system for soft-x-ray projection lithography," presented at the OSA Annual Meeting Toronto, Canada, October 3-8, 1993.

6. Ref. 14 presented at SPIE Microlithography '94, San Jose, CA, February 27 through March 4, 1994.

7. G. D. Kubiak, X-Ray Laser Applications Wkshp., Jan. 14, 1992, San Francisco, CA.(Inv.)

8. G. D. Kubiak, SPIE OELASE '92 Conference, Jan. 23 1992, Los Angeles, CA. (Inv.)

9. G. D. Kubiak, Stanford University, Elect. Eng. and Appl. Phys., May 6 1992, Stanford, CA.(Inv.)

10. G. D. Kubiak, University of Central Florida, CREOL, May 26 1992, Orlando, FL.(Inv.)

11. Ref. 1 presented at Symp. Electron, Ion, & Photon Beams, May 27 1992, Orlando, FL.

12. Refs. 3,4,5 presented at OSA Meeting on SXPL, April 8 '92, Monterey, CA.

13. G. D. Kubiak, Oak Ridge National Labs, Oak Ridge, TN, Dec. 4, 1993.

14. G. D. Kubiak, Surface Studies Seminar, LLNL, Livermore, CA, Jan. 8, 1993.(Inv.)

15. G. D. Kubiak, SDIO Dynamics of Pulsed Heating International Workshop, Los Alamos, NM, Jan. 23, 1993.(Inv.)

16. Ref. 9 presented at SPIE Microlithography meeting, San Jose, CA. March 1, 1993.

17. G. D. Kubiak, K. W. Berger, S. J. Haney, P. D. Rockett and J. A. Hunter,, Materials Research Society, San Francisco, CA, April 13, 1993.

18. Ref. 10 presented at International Conf. on Laser Ablation, Knoxville, TN, April 22, 1993 (Invited).

19. Ref. 8 presented at OSA SXPL Topical Meeting, Monterey, CA, May 11, 1993.

U.S. Patents:

5,361,292 W. C. Sweatt, "Condenser for illuminating a ring field," 11/1/94

Invention Disclosures:

TECHNICAL ADVANCE SD-5377 W.C. Sweatt, "Illuminator that couples synchrotron light into a lithographic camera with a ring field" 2/23/94

UNLIMITED RELEASE

INITIAL DISTRIBUTION

Charles W. Fowler, Jr.
U. S. Department of Energy
1000 Independence Ave., SW
DP 14
Washington, DC 20585

Frits Zernike
U.S. Department of Energy
19 Rowayton Road
Rowayton, CT 06853

Richard R. Freeman
AT&T Bell Laboratories
101 Crawfords Corner Rd.
Room 4D-437
Holmdel, NJ 07733

Dale Ibbotson
AT&T Bell Laboratories
600 Mountain Ave.
Murray Hill, NJ 07974

Sheila Vaidya
AT&T Bell Laboratories
600 Mountain Ave.
Room 2D-436
Murray Hill, NJ 07974

MS0350 Weng Chow, 1112 (10)
MS0980 Bill Sweatt, 9225 (10)
MS1436 C. E. Meyers, 1011
MS9001 J. C. Crawford, 8000
Attn: E. E. Ives, 5200
J. B. Wright, 5300
M. E. John, 8100
R. J. Detry, 8200
W. J. McLean, 8300
L. A. Hiles, 8400
P. N. Smith, 8500
L. A. West, 8600
R. C. Wayne, 8700
T. M. Dyer, 8800
D. L. Crawford, 8900

MS9161 Richard Stulen, 8342 (20)
MS9161 Glenn Kubiak, 8342 (20)
MS9161 Bill Arling, 8342
MS9161 Avi Ray-Chaudhuri, 8342
MS9161 Steve Haney, 8342
MS9406 Daniel Tichenor, 8413 (10)

MS0899 Technical Library, 13414 (4)
MS9018 Central Technical Files, 8523-2 (3)
MS9021 Technical Communications, 8535, for OSTI (10)
MS9021 Technical Communications, 8535/Technical Library, MS0899, 13414